

# The generation of optical emission-line filaments in galaxy clusters

Edward C.D. Pope<sup>1\*</sup>, Julian M. Pittard<sup>1</sup>, Thomas W. Hartquist<sup>1</sup>, Sam A.E.G. Falle<sup>2</sup>

<sup>1</sup>*School of Physics & Astronomy, University of Leeds, Leeds, UK, LS2 9JT*

<sup>2</sup>*School of Applied Mathematics, University of Leeds, Leeds, UK, LS2 9JT*

25 October 2021

## ABSTRACT

Recent data support the idea that the filaments observed in H $\alpha$  emission near the centres of some galaxy clusters were shaped by bulk flows within their intracluster media. We present numerical simulations of evaporated clump material interacting with impinging winds to investigate this possibility. In each simulation, a clump falls due to gravity while the drag of a wind retards the fall of evaporated material leading to elongation of the tail. However, we find that long filaments can only form if the outflowing wind velocity is sufficiently large,  $\sim 10^8 \text{ cm s}^{-1}$ . Otherwise, the tail material sinks almost as quickly as the cloud. For reasonable values of parameters, the morphological structure of a tail is qualitatively similar to those observed in clusters. Under certain conditions, the kinematics of the tail resemble those reported in Hatch et al.(2006). A comparison of the observations with the numerical results indicates that the filaments are likely to be a few tens of Myrs old. We also present arguments which suggest that the momentum transfer, from an outflowing wind, in the formation of these filaments is probably significant. As a result, tail formation could play a role in dissipating some of the energy injected by a central AGN close to the cluster centre where it is needed most. The trapping of energy by the cold gas may provide an additional feedback mechanism that helps to regulate the heating of the central regions of galaxy clusters and couple the AGN to the ICM.

**Key words:**

## 1 INTRODUCTION

Optical emission-line nebulae commonly surround massive galaxies in the centres of X-ray bright, cool cluster cores (Crawford et al. 1999). The origin of the H $\alpha$  filaments has been attributed to a variety of processes including: condensation from an intracluster medium (ICM) evolving as a cooling flow (Fabian et al. 1984; Heckman et al. 1989; Donahue & Voit 1991); accretion of clouds captured in galaxy mergers (Braine et al. 1995); expulsion from the central galaxy (Burbidge & Burbidge 1965).

NGC 1275 at the centre of the Perseus cluster contains the best studied example of such a nebula (Hatch et al. 2006). Its filaments are typically 50-100 pc thick and up to 30 kpc long, and the majority of them are radial. Hatch et al. (2006) presented kinematic data that rules out dynamical models of purely infalling filaments. The observed kinematic properties provide strong evidence that the filaments are not

in gravitational free fall, because, if they were, their velocities would rise sharply towards the centre of the nebula (Heckman et al. 1989). The most conclusive evidence lies in the velocity structures of the northern and northwestern filaments. The lower half of the northern filament is redshifted with respect to the galaxy, whilst the upper section is blueshifted. Thus, the upper part of the filament is flowing away from the galaxy while the lower part is flowing into the galaxy.

The filaments may follow streamlines of the flow of more tenuous material around them. In the Perseus cluster, some filaments appear to have been shaped by the wakes of the buoyant bubbles. Given that the data suggest that, at least, some parts of the filaments are outflowing, their origin may lie within the galaxy. NGC 1275 contains a large reservoir of cold molecular gas that could fuel them.

The filaments have morphologies similar to those of laminar jets, and their relatively smooth structures may place constraints on turbulent motions in the ICM. Alternatively, an ordered, amplified magnetic field trailing be-

\* E-mail:e.c.d.pope@leeds.ac.uk

hind a buoyant bubble interacting with filaments may prevent the destruction of the filaments by turbulent motions (Ruszkowski et al. 2007).

The optical nebula around NGC 1275 emits  $4.1 \times 10^{42} \text{ erg s}^{-1}$  in  $\text{H}\alpha$  and  $\text{N}[\text{II}]$ . The nature of the power source remains unclear. Various excitation mechanisms for these lines have been proposed. For instance, although ionisation by the central AGN may be important for the inner regions, it cannot be the dominant source of power for the extended nebula because the  $\text{H}\alpha$  intensity does not decrease with distance from the nucleus (Johnstone & Fabian 1988). The nebula may be excited by stellar UV, but there is no spatial correlation between the filaments and the stellar clusters. Excitation by X-rays from the ICM seems unlikely, as the ICM may be as much as a hundred times less luminous in UV than in the X-rays (Fabian et al. 2003). Heat conduction from the ICM to the colder filaments has also been proposed (Donahue et al. 2000), but it might also lead to the evaporation of the filaments on too short a timescale (Nipoti & Binney 2004). Shocks and turbulent mixing layers might play a role (Crawford & Fabian 1992). Cosmic rays, preferentially diffusing along the magnetic field lines trailing behind rising bubbles, could possibly drive the excitation in those filaments that are located in bubble wakes (Ruszkowski et al. 2007). The same magnetic fields lines could also prevent the filaments from evaporating due to thermal conduction.

The same mechanisms that power the emission could also have a profound effect on the morphology of the emitting region. It is impossible to take all of these processes into account. Consequently, we will investigate the effect of gravity and an impinging wind that strips material from a cloud on the morphology and kinematics of the resulting filament.

The main aim of the work reported here is the calculation of the density and velocity structures of material evaporated from clumps embedded in winds from the central galaxies of galaxy clusters and the comparison of model results with observations. Section 2 contains some preliminary considerations, while the model assumptions and numerical approach are treated in section 3. The simulation results appear in section 4. In section 5 we investigate the development of tails in realistic environments by including the appropriate density and gravity for a galaxy cluster. Section 6 concerns momentum transfer between clumps and the winds surrounding them. Section 7 discusses the possible trends in optical emission between clusters, and section 8 is a summary.

## 2 PRELIMINARY CONSIDERATIONS

### 2.1 Filamentary widths

We consider a clump, or cloud, embedded in a lower-density, hotter ambient wind with a speed  $v_w$  in the frame of the central galaxy. Material evaporates from the clump and interacts with the wind to form a filament.

It may be possible to estimate the age of an observed filament from its width. Previous numerical studies have shown that for a broad range of parameters the width of a filament is comparable to the diameter of the clump from which material evaporates (e.g. Dyson et al. 2006). The ra-

dius of the filament  $r_f$  would have a lower bound of approximately:  $r_f \sim 0.5c_{s,c}\Delta t$ , where  $\Delta t$  is the age of the filament, and  $c_{s,c}$  is the sound speed in the clump at the head of the filament. The length of the filament  $l_f$  would have a maximum given roughly by  $l_f \sim 2r_f v_w / c_{s,c}$ . The largest observed  $l_f / r_f$  ratios would require that  $v_w / c_{s,c} \sim 100$ s which is plausible if the clump material is molecular (and, thus, cold) before being heated to the filament temperature.

Alternatively, the width of the filament may be governed by the diffusion of material into the ICM. Consequently, it is possible to set an upper bound to the diffusion coefficient. The root mean square (RMS) displacement of a particle after time  $t$  is  $\sqrt{\langle r^2 \rangle} = \sqrt{6Dt}$ , where  $D$  is the diffusion coefficient. If the RMS displacement due to diffusion equals the measured radius of a filament, the filament's length is approximately

$$l_f \sim v_w \Delta t \sim v_w \frac{r_f^2}{6D}. \quad (1)$$

Substituting order of magnitude estimates:  $l_f = 30 \text{ kpc}$ ,  $r_f = 100 \text{ pc}$ ,  $v_w = 10^3 \text{ km s}^{-1}$  we find that  $D \sim 10^{25} \text{ cm}^2 \text{ s}^{-1}$ . Interestingly, this is comparable to the diffusion coefficients found by Roediger et al. (2007) at 30 kpc in their simulations of metal diffusion in the Perseus cluster. If diffusion were contributing significantly to filament broadening, this value of the diffusion coefficient would require the filaments to be roughly  $\Delta t \sim 5 \times 10^7 \text{ yrs}$  old.

This diffusion coefficient greatly exceeds the Spitzer thermal and viscous diffusivities. Turbulent diffusion would have to be important for such a large diffusion coefficient to obtain. The turbulent diffusion coefficient is given approximately by  $D \sim vl/3$  where  $v$  is the characteristic velocity and  $l$  the characteristic length scale of the largest eddies. If the turbulence is driven by the shear of the fluid flow past the clump and along the filament, we might assume that the thickness of the boundary layer is roughly 3% of the length of the filament (Hartquist & Dyson 1988; Canto & Raga 1991) which exceeds the observed filament widths. Therefore, a diffusion picture is not appropriate for the dynamics of the filament, but clearly viscous coupling across the entire cross section of a filament is strong, leading to a flow velocity that depends on the distance along the filament but not on the location relative to the nearest edge.

### 2.2 Clump mass-loss

The rate at which mass is ablated from a clump,  $\dot{m}$ , might be estimated by the rate at which momentum associated with the wind is transferred to the clump, divided by a speed,  $c_{s,a}$ , anywhere between the sound speed of material in the clump and the difference between the average clump speed and the average speed of material in the filament. The appropriate value of  $c_{s,a}$  depends on how effective the viscous coupling (due to turbulence or any other mechanism) between the filament material and the wind material is. The total mass lost by a clump would then be given by

$$m \approx \dot{m} \Delta t = \Delta t \frac{A \rho_w v_w^2}{c_{s,a}}. \quad (2)$$

where  $A$  is the clump cross section and  $\rho_w$  is the mass density of the wind. If  $\Delta t$  is 30 Myr, the clump has a radius  $r_c \sim 50 \text{ pc}$ ,  $\rho_w = 10^{-26} \text{ g cm}^{-3}$ ,  $v_w = 10^3 \text{ km s}^{-1}$  and

$c_{s,a} = 0.3 \text{ km s}^{-1}$ , the above equation gives  $m \sim 10^8 M_\odot$ . This is comparable to the mass of a structure with a number density of  $10 \text{ cm}^{-3}$ , radius of 50 pc, and length of 30 kpc.

### 2.3 Clump motion

A model of the clump's motion taking into account the loss of mass and the ram pressure of the impinging wind gives,

$$\frac{d}{dt}(m\dot{x}) = -m\dot{x} - mg + KA\rho_w(v_w - \dot{x})^2. \quad (3)$$

$K$  is a multiplicative factor which in the simplest case would be a constant of order unity.  $g$  is the gravitational field strength,  $x$  is the height of the clump above the central galaxy's mid-plane, and a dot indicates differentiation with respect to time. Expansion of the left-hand-side of equation (3) demonstrates that mass loss from the clump does not affect the motion of the clump. Therefore, the terminal velocity of the clump is,

$$\dot{x} = v_w - \left( \frac{mg}{KA\rho_w} \right)^{1/2}. \quad (4)$$

Using the values given above for  $\rho_w$  and  $r_c$  and taking  $g \sim 10^{-8} \text{ cm s}^{-2}$ ,  $K = 1$ , and  $m \sim 10^5 M_\odot$ , we find that  $(mg/KA\rho_w)^{1/2} \sim 10^3 \text{ km s}^{-1}$ , and so is significant for slower outflow velocities. For larger masses, and gravities, the terminal velocity is greater. The terminal velocity of the clump is not likely to be constant, because the mass of the clump falls with time. Alternatively, if the drag term is negligible, then the clump will accelerate freely, and the velocity will be given by  $\dot{x} = gt$ , if  $g$  is a constant. However, this case appears to be ruled out by observations showing slower velocities.

Since material is continually stripped from the clump as it moves relative to the surroundings, it may eventually disappear completely. Clearly, if this happens during a timescale that is less than that required for the velocity to exceed the terminal velocity, then we need not simulate the case of a clump moving at its terminal velocity. Assuming constant gravity, the free-fall time from 30 kpc is about  $10^8 \text{ yr}$  for the value of  $g$  assumed above. If the clump started from that height with zero velocity with respect to the centre of the galaxy, it will have reached a speed of roughly  $400 \text{ km s}^{-1}$  in the free-fall time. Depending on the wind parameters and gravitational field, a  $10^8 M_\odot$  molecular clump will not reach terminal velocity and may not be totally evaporated away during free fall from 30 kpc.

### 2.4 Origin of the clouds

As mention above, the data suggest that much of the material within the filaments is outflowing. There are two scenarios in which filaments with the observed properties could be produced. Firstly, clouds may form in cooling gas accreting from outside the galaxy. As they fall inwardly they would be stripped by an outflowing wind, and the lower regions of the filament could be infalling while the outer portion could be outflowing. Alternatively, such clouds may condense in gas that has been expelled from the central galaxy, and eventually begin falling back into the central galaxy as in a galactic fountain (e.g. Shapiro & Field 1976). As the clouds fall inwardly, they would be stripped by outflowing material. In

either case, an outflowing wind would ensure both infalling and outflowing portions of a filament.

### 2.5 Outflows

In a previous subsection we discussed the idea of ram pressure due to an impinging wind, or outflow. However, it is unclear how precisely how fast these winds are: the density and emission structures of transonic flows can be similar to those of nearly hydrostatic media. So, in the absence of X-ray observations with high spectral resolution, direct observational diagnosis of the kinematics is unable to distinguish firmly between low Mach number and transonic speeds. Despite this, X-ray maps do show evidence of weak shocks in the hot material at radii in the range of a few kpc to at least a few  $10^3$ 's of kpc in the Virgo and Perseus clusters (e.g. Forman et al. 2007; Sanders & Fabian 2007). Thus, we know that there are large-scale flows with transonic speeds. The sound speeds of  $3 \times 10^7 \text{ K}$  and  $10^8 \text{ K}$  ionised gas, for the Virgo and Perseus clusters, are  $8 \times 10^7 \text{ cm s}^{-1}$  and  $1.5 \times 10^8 \text{ cm s}^{-1}$ , respectively. In conjunction with the X-ray maps, this suggests that the wind speeds are likely to be  $\sim 10^8 \text{ cm s}^{-1}$ . In fact, we suspect that the flows may be fountain-like and that outwardly flowing gas eventually falls back inwards. As a result, the wind velocity is not constant, but drops off with radius. So by the time it reaches the cold clouds the wind velocity will be much reduced from its central value.

AGN activity is considered a prime candidate for preventing the ICM cooling from  $10^8 \text{ K}$  at rates of more than  $100 M_\odot \text{ yr}^{-1}$ . This requires an energy input rate of  $10^{44} \text{ erg s}^{-1}$  which is comparable to the kinetic energy flux of material with a mass density of  $2 \times 10^{-26} \text{ g cm}^{-3}$  flowing through a spherical surface of radius 10 kpc with a radial velocity of  $10^8 \text{ cm s}^{-1}$ . Thus, the ‘‘cooling problem’’ and our wind speed estimates imply comparable power inputs from AGN.

The outflows we envisage would probably be somewhat, although not hugely, collimated. X-ray images of the centre of the Perseus cluster show some asymmetry in structures at radii approaching 10 kpc. Outside about 10 kpc, the interaction of AGN plasma with ambient galactic interstellar and intracluster gas appears to reduce asymmetries associated with collimated AGN outflows. The filaments extend several times this far in radii, and are radial suggesting that the wind may be fairly isotropic at such radii.

One would also expect the outflows to be somewhat time-dependent. However, the presence of clouds dotted throughout the ICM may well have the effect of obstructing the outflow of energy injected by the AGN. Therefore, the time-variability of the AGN-driven flow far away from its source is likely to be fairly uncorrelated with the variability at the source. Essentially this means that, although the initial energy injection rate may be time-variable, at larger radii the variations may have been smoothed-out making the flow relatively steady. Finally, intermittency on long timescales much greater than  $3 \times 10^7 \text{ yr}$  will be on timescales greater than the ages of the structures we are attempting to explain, and consequently unimportant in this work. Based on these considerations, we will assume the outflows to be transonic, isotropic and steady.

### 3 NUMERICAL SETUP

#### 3.1 Assumptions and methods

We use hydrodynamical simulations to investigate the interaction between a tenuous flow and a mass source. The source of mass is assumed to be a cold cloud from which material is stripped due to the interaction with an incident wind. The basic approach is similar to that adopted by Falle et al. (2002), Pittard et al. (2005), and Dyson et al. (2006). The main difference is that here we also include the effects of gravity to make the model more appropriate for a typical galaxy cluster environment.

Despite including the gravitational potential, we will ignore self-gravity for this set of simulations, for the following reasons. Self-gravity is certainly important in the cold clump at the bottom of each filament, and would be important in our model if we were to try to calculate the mass loss rate of the clump. As we have already stated, the details of the injection process are not important for the question we are addressing. Self-gravity may well be important in the filaments, but the absence of a population of bright, young stars associated with the filaments (e.g. Hatch et al. 2006) also provides some evidence that it may not. As an illustration, we give the ratio of the magnitude of the gravitational field to the magnitude of the thermal pressure force per unit volume in a cylindrical filament of mass density  $\rho$  and radius  $R$  is approximately,

$$\frac{g\rho R}{P} = \frac{2\pi G\rho\mu m_p R^2}{k_b T} \approx 0.3 \left( \frac{\rho}{10^{-22} \text{ g cm}^{-3}} \right) \left( \frac{R}{30 \text{ kpc}} \right)^2 \left( \frac{T}{10^4 \text{ K}} \right)^{-1}, \quad (5)$$

where  $\mu m_p$  is the mean mass per particle in the gas. Thus, filament parameters are in the range that may allow the ratio to approach unity. However, it is clear that the values are sufficiently uncertain that an initial focus on cases in which self-gravity is neglected is reasonable. Furthermore, if self-gravity does lead to instability, shear may limit the development of clumps. We will neglect self-gravity for the present investigation.

The simulations are split into two groups. In the first we assume constant gravity, and work in the frame of the cloud. This is to gain an understanding of the effect of the gravitational potential and the density contrast between the cloud and the wind. In the second group, we employ a realistic cluster atmosphere and work in the rest frame of the cluster, and advect the cloud. This allows us to implement what we have learnt from the prior simulations in the more realistic case. The latter setup is discussed more fully in section 6. In either case, the velocity of the incident wind increases, as measured in the clump frame, with time. Gravity also affects the motion of material in the tail.

For all models we assume a rate of mass injection per unit time and volume that may vary temporally, but that is spatially uniform within a given radius of the cloud's centre. This mass injection prescription is simple to implement, but has the disadvantage that the flow from the injection region is isotropic. However, the effect of asymmetric mass loss is small at large distances from the cloud (Pittard et al. 2005). Therefore, we emphasize that the actual details of the mass injection process are relatively unimportant. The boundary

of the mass injection region is not meant to coincide with the boundary of a cloud, and the cloud could be much smaller than the injection region.

Three-dimensional calculations are required if the sources are spherical. To reduce the computational cost we restrict ourselves to two-dimensional simulations in which the sources are cylindrical. While we expect some differences between calculations performed in two and three dimensions, at this stage we can still gain important insight from less computationally demanding two-dimensional simulations.

In this study we treat the hot gas as adiabatic, since in the Perseus cluster the cooling time of X-ray emitting gas at 30 kpc is  $\sim 10^9$  yr, much longer than the flow time of the outflow along the tail. The cooling rate of the gas in the tail itself is very high, and must obviously be offset by a heating rate. We do not know the precise temperature of this gas, but the optically emitting gas in the tail is at about  $10^4$  K. An isothermal treatment of this material is reasonable. Thus, we investigate the simple case in which the incident wind behaves adiabatically, while the injected gas remains isothermal.

To ensure isothermal behaviour, we use an advected scalar,  $\alpha$ , which is unity in the injected gas and zero in the ambient gas. The source term in the energy equation is then

$$\kappa\alpha\rho(T_0 - T), \quad (6)$$

where  $\rho$  and  $T$  are the local mass density and temperature, and where  $\kappa$  is large enough that the temperature always remains close to the equilibrium temperature,  $T_0$ , in the injected gas. Inside the injection region we added an extra energy source so that the gas is injected with temperature  $T_0$  (see Falle et al. 2002, for further details).

The simulations are performed using *mg\_gt*, a second-order accurate code with adaptive mesh refinement (AMR). *mg\_gt* uses a hierarchy of grids  $G^0 - G^N$  such that the mesh spacing on grid  $G^n$  is  $\Delta x_0/2^n$ . Grids  $G^0$  and  $G^1$  cover the whole domain, but the finer grids only exist where they are needed. The solution at each position is calculated on all grids that exist there, and the difference between these solutions is used to control refinement. In order to ensure Courant number matching at the boundaries between coarse and fine grids, the time-step on grid  $G^n$  is  $\Delta t_0/2^n$  where  $\Delta t_0$  is the time-step on  $G^0$ .

In this model, we are studying the behaviour of cold clouds located  $\sim 10$  kpc away from the centre of the cluster. At such distances, the gravitational acceleration in galaxy clusters is  $\sim 10^{-7} \text{ cm s}^{-2}$ . We investigate different density contrasts between the cloud material and the ambient gas, and compare the morphology of the results with observations.

#### 3.2 Variables

The problem we are investigating is scale-free. For numerical reasons, we have chosen scales so that the values of parameters are near unity. For easier comparison with the astrophysical systems of interest we will rescale the results to physical units. In particular, we have scaled the length by a factor  $L$ , the gravitational acceleration by  $G$ , and the density by  $R$ . In this case, the hydrodynamic quantities scale

as,

$$x = Lx', \quad (7)$$

$$g = Gg', \quad (8)$$

$$\rho = R\rho', \quad (9)$$

$$t = \tau t' \quad (10)$$

$$v = \frac{L}{\tau} v', \quad (11)$$

$$p = R \left( \frac{L}{\tau} \right)^2 p', \quad (12)$$

where the primed quantities represent the dimensionless simulation values, and the unprimed quantities represent the real values.  $t$  is time,  $v$  is velocity, and  $p$  is pressure. In cases in which  $g$  is nonzero

$$\tau = \sqrt{\frac{L}{G}} \quad (13)$$

In our simulations the values selected for parameters are roughly consistent with estimates of the properties of clouds in the Perseus cluster: the length  $L = 50$  pc,  $G = 10^{-7} \text{ cm s}^{-2}$  (except for one case) and  $R = 10^{-23} \text{ g cm}^{-3}$ . For cases in which  $g = 0$ , we leave  $\tau = 1.24$  Myrs, which is the same value as when  $g$  is nonzero. In section 5, we have employed more accurate values of the scaling factors.

### 3.3 Initial conditions

To ensure that the ambient wind does not penetrate the injection region, we take the ram pressure of the injected material at the boundary of the injection region to be larger than that of the wind, i.e. we require,

$$v_i^2 \rho_i = \frac{v_i r_i Q}{3} \geq \rho_w v_w^2, \quad (14)$$

where  $r_i$  is the radius of the injection region,  $v_i$  is the flow speed of the injected material at  $r = r_i$  and  $\rho_i$  its density at this point.  $Q$  is the rate per unit volume per unit time at which mass is injected within  $r = r_i$ .

If we use the pressure behind a stationary normal shock in the wind rather than the wind's ram pressure, the above criterion becomes

$$Q \geq \frac{4}{\gamma + 1} \frac{\rho_w v_{w,0}^2}{v_i r_i}. \quad (15)$$

In the frame of a falling clump, the wind's ram pressure increases with time. Thus, the minimum mass injection rate must increase accordingly to ensure that the wind does not penetrate the injection region. If the value of  $Q$  at  $t = 0$  is  $Q_0$  and the gravity is constant, the ratio of  $Q$  to the wind ram pressure will remain constant if

$$Q = Q_0 \left( 1 + \frac{gt}{v_{w,0}} \right)^2, \quad (16)$$

where  $v_{w,0}$  is the relative velocity between the clump and the ambient flow at  $t = 0$ . While the method that we are using to treat mass injection requires that we take  $Q$  to increase

with time, in reality the mass injection rate will increase with ram pressure (e.g. Hartquist & Dyson 1988).

The computational domain is  $-200 \leq x \leq 200$ ,  $-100 \leq y \leq 400$ , with the mass injection region centred at the origin. We use 6 grids, and the size of the finest cells is 0.125.

By scaling the physical variables we can choose units such that  $r_i = 1$ ,  $v_i = 1$ , and  $\rho_w = 1$  and initially set  $v_w = 10$  and  $T_0 = 1$ . Furthermore, we assume that the injected material is in pressure equilibrium with the ambient wind. Thus, if we assume that the injected material is a factor of  $10^3$  cooler than the ambient wind, then it is also  $10^3$  times denser than the wind. We will use  $\eta$  to represent this contrast parameter.

We investigate the morphology of tails for three different contrast parameters:  $\eta = 10^2$ ,  $10^3$ , and  $10^4$ . The corresponding initial values of the adiabatic Mach number,  $M$ , are: 0.77, 0.24, and 0.077, respectively. These parameters define case 1), 2), and 3), respectively. Clearly, as the ambient wind accelerates with respect to the cloud, the Mach number will increase.

For comparison, we also study several other cases in which the density contrast is  $10^3$ . Case 2i) is identical to case 2) except that  $g' = 10$  and  $G = 10^{-8}$ . In cases 2ii) and 2iii) the gravity is zero, but there is a constant wind velocity of 10 and 30 (in code units) respectively, corresponding to Mach numbers of 0.24 and 0.72. These parameters are summarised in table 1. It does not make sense to specify the mass of the clouds, since they are likely to be composed partly of molecular material, and therefore considerably more massive than an estimate of  $4\pi r_c^3 \rho_c / 3$  would suggest.

The code wind velocity  $v'_w = 10$ , corresponds to a velocity of  $v_w = 3.9 \times 10^7 \text{ cm s}^{-1}$ , which, is comparable with the transonic values described in the previous section.

### 3.4 Sub-grid turbulence model

Simulations with a transonic wind pose difficulties that are absent in those for hypersonic winds. Firstly, in order for the boundaries to have no effect on a simulation with a transonic wind, the computational domain has to be very large. Secondly, the velocity shear between the injected material and the wind is so extreme in the transonic case that the wind flow separates and produces a turbulent wake downstream of the interaction region. Calculations based on the Euler equations cannot adequately describe such turbulence, and a turbulence model must be employed.

We adopt the  $k - \epsilon$  model used by Falle et al. (2002). The subgrid turbulence model allows the simulation of a high Reynolds number flow through the inclusion of equations for the turbulent energy density and dissipation rate, from which viscous and diffusive terms are calculated. The model solution gives an approximation to the mean flow. The diffusive terms in the fluid equations model the turbulent mixing of the injected gas with the original flow due to shear instabilities. The model has been calibrated by comparing the computed growth of shear layers with experiments (Dash & Wolf 1983). It is based on the assumptions that the real Reynolds number is very large, which is the case in astrophysical flows, and that the turbulence is fully developed. The use of the subgrid model gives more realistic results than those obtained from a hydrodynamical code where the sizes of the shear instabilities are determined by

**Table 1.** Simulation parameters: ambient density, cloud density, sound speed of injected material, initial Mach number of the wind velocity with respect to cold material, gravitational acceleration. The implied mass outflow rates close to the origin are  $4\pi r^2 \delta \rho_{\text{amb}} v_w \sim 10 M_{\odot} \text{ yr}^{-1}$ , where  $\delta \sim 0.1$  is the fraction of the sky covered by the outflow.

| Case | $\rho_{\text{amb}} (g \text{ cm}^{-3})$ | $\rho_c (g \text{ cm}^{-3})$ | $c_{s,c} (\text{cm s}^{-1})$ | $M_{\text{initial}}$ | $g (\text{cm s}^{-2})$ |
|------|---|------------------------------|------------------------------|----------------------|------------------------|
| 1    | $10^{-26}$                              | $10^{-24}$                   | $5.2 \times 10^5$            | 0.77                 | $10^{-7}$              |
| 2    | $10^{-26}$                              | $10^{-23}$                   | $1.6 \times 10^5$            | 0.24                 | $10^{-7}$              |
| 3    | $10^{-26}$                              | $10^{-22}$                   | $5.2 \times 10^4$            | 0.077                | $10^{-7}$              |
| 2i   | $10^{-26}$                              | $10^{-23}$                   | $1.6 \times 10^5$            | 0.24                 | $10^{-7}$              |
| 2ii  | $10^{-26}$                              | $10^{-23}$                   | $1.6 \times 10^5$            | 0.24                 | $10^{-7}$              |
| 2iii | $10^{-26}$                              | $10^{-23}$                   | $1.6 \times 10^5$            | 0.72                 | $10^{-7}$              |

the numerical resolution. Further details can be found in Falle (1994).

## 4 RESULTS

### 4.1 Morphology

In general, the morphologies of the filament density generated by accelerating flows are very similar to those presented in Pittard et al. (2005). A bow wave develops upstream of a mass source, and the wave's amplitude falls off as  $1/r$ . If the flow becomes supersonic, the bow wave becomes a bow shock and a very weak tail shock may occur in the wind downstream of the mass source, when the external flow is subsonic. The injected material remains in approximate pressure equilibrium with the wind, and eventually becomes confined to a tail with a width comparable to that of the injection region (cf. figures 1 to 4). The opening angle of the injected material increases with the external Mach number.

It should be noted that we use a sub-grid turbulence model which, in effect, models a turbulent boundary layer at the surface of the filament. So even when the tail appears smooth there is significant turbulence. For increasingly large density contrasts, the turbulent viscosity, which is an integral part of the subgrid turbulence model, fails to stabilize the subsonic shear layer. In this case, there is turbulence on the grid as well as sub-grid turbulence. Large-scale instabilities in thin filaments demand high density contrasts and an ambient flow that remains subsonic with respect to the clump.

The opening angle of a turbulent boundary layer is given by Canto & Raga (1991) as,

$$\frac{dh}{dx} = \frac{2}{\sigma} \quad (17)$$

where  $\sigma$  is the so-called spreading parameter. Experiments show that at low Mach number, turbulent mixing layers have a constant opening angle, and  $\sigma \sim 11$ , so that  $dh/dx \sim 10.4$ . At high Mach numbers,  $\sigma \sim 50$ , so  $dh/dx \sim 2.3$ . The tail becomes fully turbulent at a downstream distance of,

$$x = \frac{r_c M_w c_0}{2\epsilon c_w} \quad (18)$$

where  $\epsilon$  is the entrainment efficiency,  $M_w$  is the Mach number of the wind with respect to the clump,  $c_{s,a}$  is the sound speed of the environment,  $c_{s,c}$  is the sound speed of the tail material,  $r_c$  is the initial radius of the tail.

To calculate this length, Canto & Raga use  $x = 16.9 M_w r_c$ , which can be rescaled as,

$$x \approx 0.85 \text{ kpc} \left( \frac{M_w}{1} \right) \left( \frac{r_c}{50 \text{ pc}} \right), \quad (19)$$

in other words, for sensible values of the wind flowing past a clump, we should expect the tail to be turbulent on kpc scales.

These figures show a clear dependence, at least at early times, of the tail morphology on the density contrast between the cloud and the ambient gas. For example, for  $\eta = 10^4$  (figure 3), the tail is nearly linear, but is punctuated by fairly evenly spaced blobs along the length of the tail. This is because subsonic shear layers tend to be unstable unless the viscosity is high. Some turbulent jets display similar behaviour. The blobs are separated by increasingly large distances further along the tail, indicating acceleration. For  $\eta = 10^2$ , (figure 1) the tail only becomes irregular at large distances away from the cloud, while for  $\eta = 10^3$  (figure 2) most of the tail is irregular. For comparison we also show the morphologies for a case when the gravity is weaker (figure 4) and nongravitational cases with different ambient flow velocities (figures 5 and 6).

For ambient flows that remain subsonic in the frame of the clumps, the tails are irregular in appearance. In case 2i) the gravity is strong enough that the initially subsonic flow becomes supersonic, and consequently the tail becomes smooth and regular. Morphological considerations by themselves would suggest that the filaments in the Perseus cluster satisfy these conditions. However, an examination of the kinematic structures of the model and observed filaments is also necessary.

### 4.2 Velocity profiles

Figures 7 to 10 show the mean velocity of the tail material at 100 increments along the length of the tail for each of cases 1), 2), 3), and 2i).

Except for case 2i) and to some extent case 1), each velocity profile shows some scatter around a mean velocity that is roughly constant along the length of most of the filament. We do not show velocity profiles for cases 2ii) and 2iii) because they show behaviours similar to those for cases 2) and 3). However, the velocity profiles, including those for the model filaments that bear the most morphological resemblance to the observed filaments, are not compatible with the observed velocity structures of the NGC 1275 filaments. Nevertheless, the third panel of figure 10 shows clear

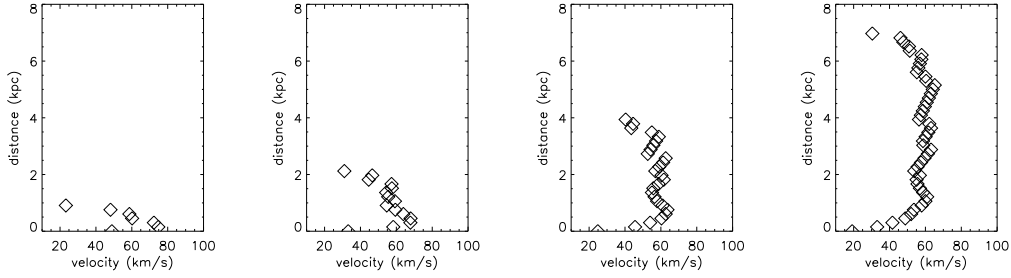


**Figure 7.** Velocity profile for case 1) for (from left to right)  $t' = 6.95, 14.5, 20.9,$  and  $28.2$  ( $t = 8.3, 18, 26,$  and  $35$  Myrs), respectively. The Mach numbers of the ambient flow with respect to the cold clump are: 1.3, 1.9, 2.4, and 3, respectively. We have removed the central  $10 \text{ km s}^{-1}$  to avoid any points where the tail does not exist.

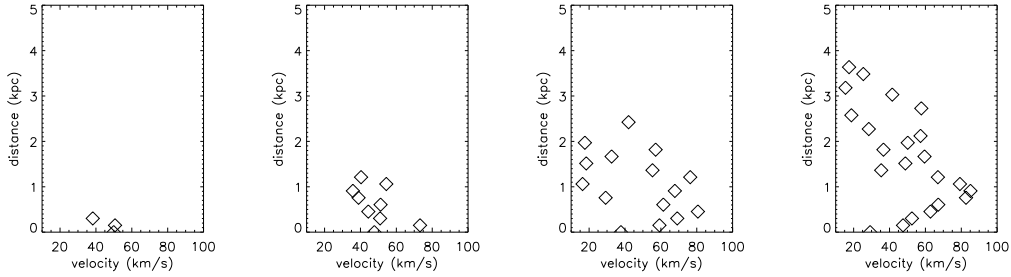


**Figure 8.** Velocity profile for case 2) for  $t' = 3.4, 8.3, 12.1,$  and  $16.9$  ( $t = 4.3, 10, 15,$  and  $21$  Myrs) respectively. The Mach numbers of the ambient flow with respect to the cold clump are 0.33, 0.45, 0.54 and 0.66, respectively. We have removed the central  $10 \text{ km s}^{-1}$  to avoid any points where the tail does not exist.

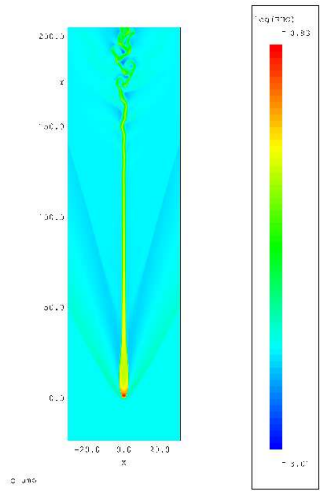


**Figure 1.** Density morphology for case 1) at  $t' \approx 28$  ( $t \approx 35$  Myrs) at which time the external flow at the position of the clump has accelerated to  $M = 3$ . The initial Mach number was 0.77. Each spatial unit corresponds to 50 pc. Thus, the plotted domain, in the x-direction, extends between  $\pm 1.5$  kpc. The density contrast between the cold clump and the ambient gas is  $10^2$ . Note the bow shock around the clump, and also the tail shock behind this.

zig-zag features, which are similar to those in the velocity profiles given in figures 5, 7 and 14 of Hatch et al. (2006). Note that the zig-zag features in figures 7 and 10 also correspond to the regions of enhanced density along the tail. The similarity between figures 7 and 10 suggests that the zig-zag

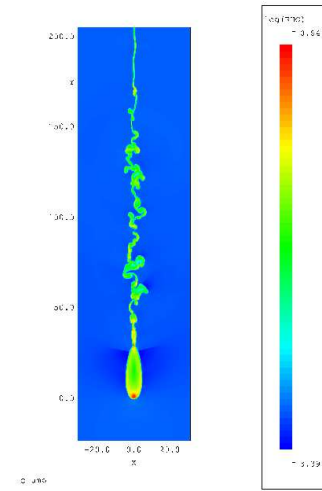


**Figure 2.** Density morphology for case 2) at  $t' \approx 17$  ( $t \approx 21$  Myrs) when  $M = 0.66$ . The initial Mach number was 0.24. The density contrast between the cold clump and the ambient gas is  $10^3$ . Note the irregular structure of the tail along the entire length of the filament, compared to the linear tail in the previous figure.

features occur when the Mach number of the ambient flow, with respect to the clump, is roughly 2-3, after  $\sim$  few 10s Myrs.

The velocities near the heads of the model filaments are low, whereas those of the observed filaments are not. The discrepancy could be due to the material near the heads of the observed filaments being warm, but neutral, and hence

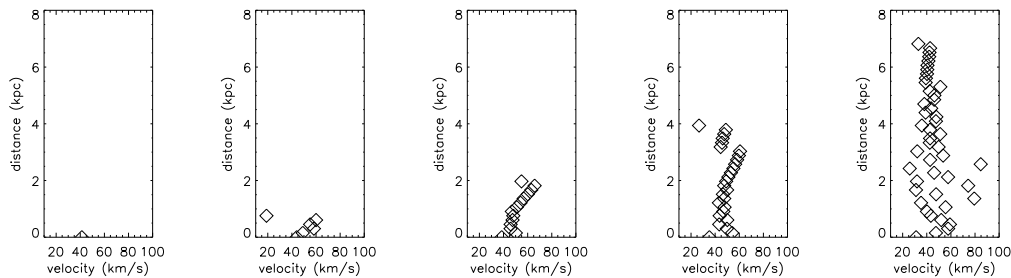


**Figure 9.** Velocity profile for case 3) for  $t' = 1.93, 5.7, 12.7$  and  $18.1$  ( $t = 2.4, 7.0, 12,$  and  $22$  Myrs) respectively. The Mach numbers of the ambient flow with respect to the cold clump are  $0.09, 0.12, 0.15, 0.18$  and  $0.22$ , respectively. We have removed the central  $10 \text{ km s}^{-1}$  to avoid any points where the tail does not exist.

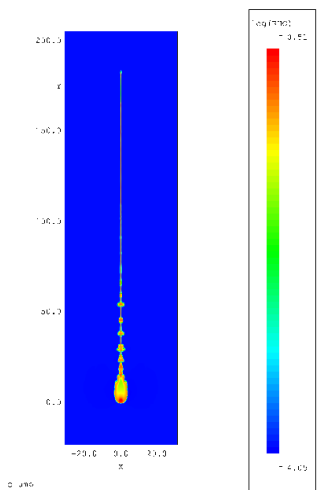


**Figure 3.** Density morphology for case 3) at  $t' \approx 18$  ( $t \approx 22$  Myrs) when  $M = 0.22$ . The initial Mach number was  $0.077$ . The density contrast between the cold clump and the ambient gas is  $10^4$ . Note the approximately linear tail, with at least 6 discrete blobs of material close to the clump.

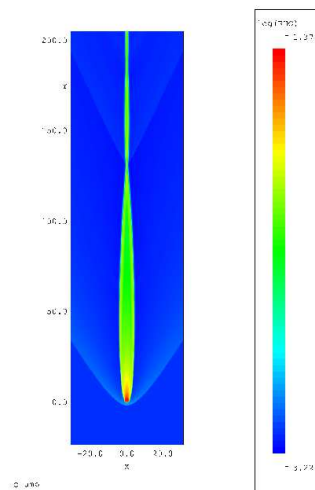


**Figure 4.** Density morphology for case 2i) at  $t' \approx 20$  ( $t \approx 25$  Myrs) when  $M = 5.2$ . The initial Mach number is  $0.24$ . The density contrast between the cold clump and the ambient gas is  $10^3$ . The structure of the tail in this example is regular, with no obvious blobs at various locations along the tail.

invisible in the observed optical lines. More likely, it is a result of our prescription for mass injection which will produce different features near the injection region, but the large-scale downstream flow should be unaffected.

The fact that the profile shown in figure 10 resembles the observed profile better than that shown in figure 7, is probably because the density contrast between the cold clump and the ambient flow is more realistic in case 2i). It is likely that if we had continued simulating cases 2) and 3) to high enough Mach numbers that they may also have begun to exhibit the zig-zag structure. Based on these results it appears that the velocity fluctuations (and scale-size of instabilities) are larger for greater density contrasts between the clump and the wind.

## 5 TAILS IN A REALISTIC CLUSTER ENVIRONMENT: THE PERSEUS CLUSTER

Having investigated the properties of accelerating flows past cold clouds, we now study the more specific case of a galaxy cluster atmosphere. Firstly, we assume a generic gravita-

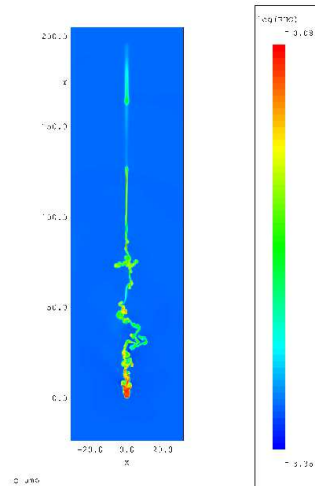


**Figure 5.** Density morphology for case 2ii) at  $t' \approx 20$  ( $t \approx 25$  Myrs). The density contrast between the cold clump and the ambient gas is  $10^3$ , and gravity is omitted from the simulation.  $M = 0.24$ .

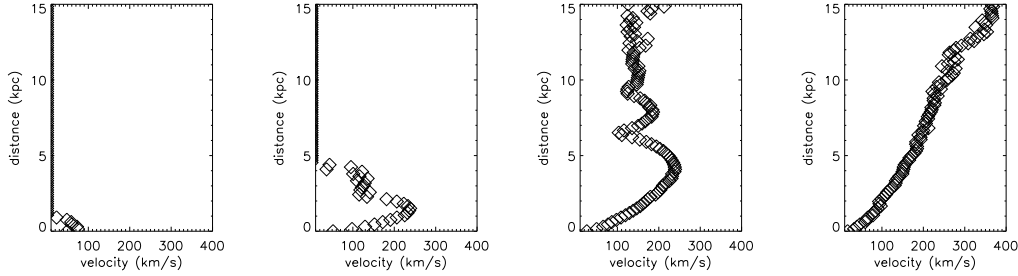


**Figure 10.** Velocity profile for case 2i) at  $t' = 2, 5, 10,$  and  $20$  ( $t = 2.5, 6.2, 12,$  and  $25$  Myrs), respectively. The Mach numbers of the ambient flow with respect to the cold clump are 0.74, 1.5, 2.7 and 5.2, respectively. We have removed the central  $10 \text{ km s}^{-1}$  to avoid any points where the tail does not exist.

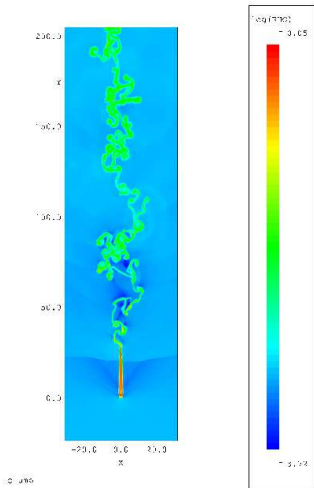


**Figure 6.** Density morphology for case 2iii) at a code time of  $t' \approx 20$  ( $t \approx 25$  Myrs). The density contrast between the cold clump and the ambient gas is  $10^3$ . Gravity is omitted from this simulation.  $M = 0.72$ .

tional potential which leads to a  $\beta$ -profile gas density profile in hydrostatic equilibrium (e.g. Vignelli & Reynolds 2006),

$$\rho = \frac{\rho_0}{[1 + (r/r_0)^2]^\beta}, \quad (20)$$

where we have assumed spherical symmetry,  $r$  is the radial coordinate, and  $r_0$  is the scale-height of the density distribution. The gravitational acceleration is therefore given by

$$g = -2\beta \frac{k_b T}{\mu m_p} \left( \frac{r}{r_0^2 + r^2} \right), \quad (21)$$

where  $T$  is the gas temperature which is assumed to be constant with radius,  $\mu = 0.6$  is the mean mass per particle.

For each such model, we will perform the calculations in the frame of the central galaxy and prescribe how the cloud injection region moves. Due to the structure of the gravitational potential employed and the initial location assumed for the cloud, the solution of the cloud motion is very close to that for free-fall. Assuming free-fall, we find that the velocity, after starting from rest at  $x_0$ , is,

$$v(r) = - \left( 2\beta \frac{k_b T}{\mu m_p} \right)^{1/2} \left[ \frac{r_0^2 + x_0^2}{r_0^2 + r^2} \right]^{1/2}. \quad (22)$$

Equation (22) can be numerically integrated, using the

values for specific galaxy clusters, to obtain the position of the cloud at each point in time,  $r(t)$ . For example, for the Perseus cluster we use,  $T = 10^8 \text{ K}$ ,  $\rho_0 = 7 \times 10^{-26} \text{ g cm}^{-3}$ ,  $\beta = 0.81$ , and  $r_0 = 28.5 \text{ kpc}$  (e.g. Pope et al. 2006). With these values, the motion of a cloud falling freely from 30 kpc can be well approximated by,

$$r(t) = 30 \left[ 1 - 0.9 \left( \frac{t}{75 \text{ Myr}} \right)^2 \right] \text{ kpc}, \quad (23)$$

which is roughly what one would expect for constant gravity. This correspondence occurs because the gravitational acceleration scales as  $1/r$  at large radii, and  $r$  at small radii. The cloud is initially located around the turning point where the function is relatively flat. This means that constant gravity is a suitable approximation and the previous set of simulations, in which constant gravity was assumed, retain their validity.

For completeness, the Mach number of the flow around the clump, with respect to the ambient flow, is

$$M = \frac{2\beta}{\gamma^{1/2}} \left( \frac{r_0^2 + x_0^2}{r_0^2 + r^2} \right). \quad (24)$$

Thus, for  $\beta = 3/2$ ,  $r_0 = 28.5$ ,  $x_0 = 30 \text{ kpc}$ , we find that  $M > 1$  for  $r \lesssim 0.9r_0 \approx 26 \text{ kpc}$ . Consequently, for higher wind velocities, the flow becomes supersonic closer to the initial location,  $x_0$ . The ram pressure due to relative motion between the cloud and the static atmosphere is,

$$\rho_w v_w^2 = \rho [r(t)] \left[ \frac{dr(t)}{dt} \right]^2. \quad (25)$$

We choose an initial density contrast between the cloud and its surrounding of  $10^4$ , and set the scaling parameters to  $R = 7 \times 10^{-22} \text{ g cm}^{-3}$  and  $L = 3.085 \times 10^{21} \text{ cm}$ .  $P = \rho k_b T / \mu m_p \approx 3.6 \times 10^{-10} \text{ erg cm}^{-3}$  in the centre of the Perseus cluster, giving  $G = P / (P' R L) = 1.66 \times 10^{-10} \text{ cm s}^{-1}$ . The temporal scaling constant, is  $\tau = 4.3 \times 10^{15} \text{ s}$ , while the velocities are scaled by  $L/\tau = 7.2 \times 10^5 \text{ cm s}^{-1}$ . The time taken for the cloud to fall from 30 kpc to 3 kpc is 75 Myr, or 0.55 in terms of code time units. For a density contrast of  $10^3$ , we use  $R = 7 \times 10^{-23} \text{ g cm}^{-3}$  and  $L = 3.085 \times 10^{21} \text{ cm}$ , giving  $G = 1.66 \times 10^{-9} \text{ cm s}^{-1}$ . This means that the temporal scaling constant becomes  $\tau = 1.4 \times 10^{15} \text{ s}$ , and the velocities are scaled by  $L/\tau = 2.2 \times 10^6 \text{ cm s}^{-1}$ . The time taken for the cloud to fall from 30 kpc to 3 kpc now, or 1.7 in terms of code time units.

Finally, in the preliminary simulations we found that

the tail widths were comparable to the diameters of the clouds. Therefore, to generate filaments of the observed widths which are constrained to be  $<1$  kpc we will simulate the effect of material stripped from relatively large clouds, with an injection region of radius 100 pc. As already stated this may be significantly larger than the physical size of the cloud.

### 5.1 Results

Since the lateral velocity dispersion (zig-zag effect) appears to increase for larger density contrasts, we will concentrate on the case  $\eta = 10^4$ . However, the case where  $\eta = 10^3$  is also of interest. The general properties are as follows: long tail-like structures only form if the wind velocity is sufficiently large. This wind is assumed to be the same material, at the same temperature as the static atmosphere. For example, for low values of  $v'_w$  (5 and 10, corresponding to  $3.6 \times 10^6$  and  $7.2 \times 10^6$   $\text{cm s}^{-1}$  for  $\eta = 10^4$ ), the tail never becomes long because the ram pressure due to the impinging wind cannot overcome the gravitational force acting on the tail material. As a result any tail that forms is infalling everywhere, which contradicts the observational data, at least for NGC 1275. It therefore appears that the length and morphology of the tails are extremely dependent on the wind velocity.

The morphology of the tail also depends strongly on the density contrast between the cloud and its environment. In each figure, the cloud is shown as red and is the lowest point along the line defined by  $x=0$ . Material is injected (stripped) and collects behind the free-falling cloud, and some dense material sinks either side of the cloud. Behind this cold material, a filamentary tail forms. Inhomogeneities in the tails are dependent on the wind speed and density contrast, in agreement with the previous results. As can be seen from figures 11 to 14, it appears that a density contrast of  $\eta = 10^3$  produces structures most qualitatively similar to those seen in real filaments. However, they are low density, being a few  $\times 0.1$  particles per cubic centimetre. This does not present problems in terms of pressure balance between the tail and the ambient medium since the tail material is diluted and heated to temperatures in the range  $10^5 - 10^7$  K. The simulations produce filaments of  $10^6 - 10^7 M_\odot$  while the estimates in the following section suggest that  $10^8 M_\odot$  filaments might be more likely. Even so, the quantity of cold gas, in the simulated tail, is more than capable of producing the observed optical luminosity (see Hatch et al. 2007, for example).

The material around the head of the cloud also exhibits different behaviour in this set of simulations. Material is stripped from the cloud by the wind and builds up behind. It appears that in many cases much of this material does not make it into a tail but simply collects behind the cloud. Eventually this becomes unstable, probably due to Rayleigh-Taylor instabilities, and produces the structures seen in the simulations. Similar structures have been noticed in previous numerical simulations in the work by Murray & Lin (2004).

In the simulations, initial wind velocities of  $\sim 10^8$   $\text{cm s}^{-1}$  are required to produce long tails which are out-flowing at their outer extent. This large velocity is expected, since the velocity of the wind, at the clump, must exceed the infall velocity of the clump for material to be carried away from it. By the time the wind has reached the clump it has

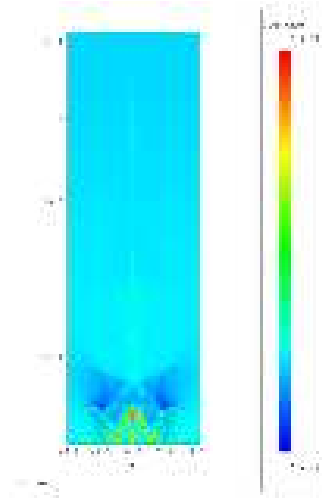


**Figure 11.** The density structure at 58 Myrs, for  $\eta = 10^4$  and wind velocity =  $5.8 \times 10^7$   $\text{cm s}^{-1}$ . Panel shows data at  $3.4 \times 10^7$  yrs. The length scale indicates the distance from the cluster centre in kpc. The density scale shows the density in code units ( $\rho'$ ).

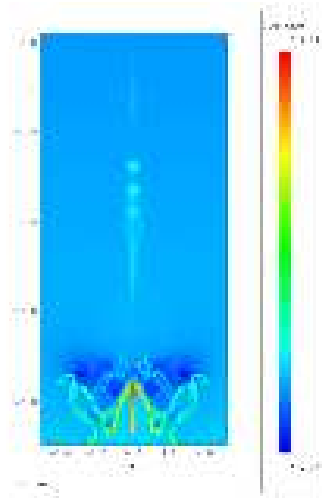
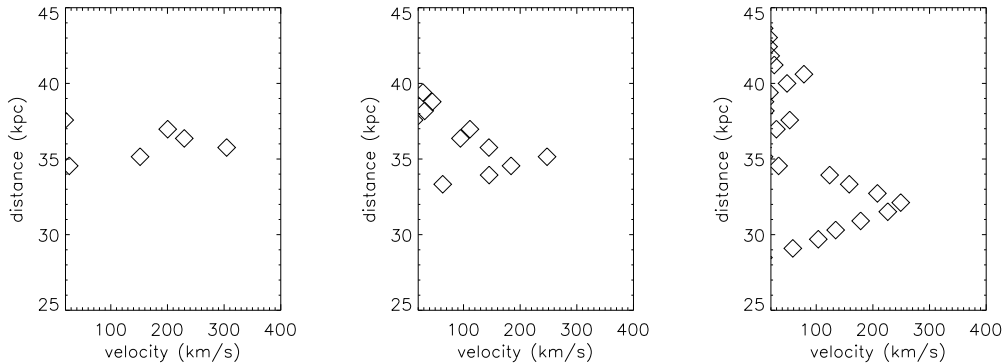


**Figure 12.** The density structure at 38 Myrs, for  $\eta = 10^4$  and wind velocity =  $4.32 \times 10^8$   $\text{cm s}^{-1}$ . The length scale indicates the distance from the cluster centre in kpc. The density scale shows the density in code units ( $\rho'$ ).

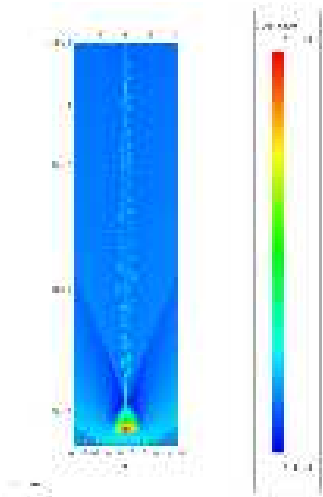
done considerable work against gravity. This leads to the velocity dispersion along the clump of a few  $\times 100$   $\text{km s}^{-1}$ .

Figure 15 shows the velocity profile for  $\eta = 10^4$  and a wind speed of  $5.8 \times 10^7$   $\text{cm s}^{-1}$  ( $v'_w = 80$ ). This case probably best resembles the observations. Figure 16 seems to show that a lower wind velocity ( $v'_w = 60$ ,  $v_w = 4.32 \times 10^7$   $\text{cm s}^{-1}$ ) does not produce the observed zig-zag kinematics for this particular density contrast. These results should be compared with the  $\eta = 10^3$  case.

Figures 17 and 18 show the kinematics for two wind velocities:  $v'_w = 80$  and 60, in figures 17 and 18. These correspond to  $1.76 \times 10^8$   $\text{cm s}^{-1}$  and  $1.32 \times 10^8$   $\text{cm s}^{-1}$  which are either side of the sound speed of the ambient medium ( $1.52 \times 10^8$   $\text{cm s}^{-1}$ ). Figure 18 eventually shows kinematic



**Figure 15.** Velocity profile for case  $\eta = 10^4$  and wind velocity  $= 5.8 \times 10^7 \text{ cm s}^{-1}$ . Panels show data at 14, 21 and 34 Myrs. The length scale indicates the distance from the cluster centre. We have cut off the central  $20 \text{ km s}^{-1}$  to exclude points where there is no tail.



**Figure 13.** The density structure at 20 Myrs, for  $\eta = 10^3$  and wind velocity  $= 1.76 \times 10^8 \text{ cm s}^{-1}$ . The length scale indicates the distance from the cluster centre in kpc. The density scale shows the density in code units ( $\rho'$ ).

structure that could be interpreted as a zig-zag, although it is not as clear as in figure 15. The tails extend to greater lengths for  $\eta = 10^3$  than  $\eta = 10^4$  because the evaporated material is less dense and can be more easily transported outwards by the wind.

Again, the amplitude of the zig-zags is smaller for  $\eta = 10^3$  than  $\eta = 10^4$ . As a result, these simulations suggest that a density contrast between the cold material and the ICM of  $10^4$  is a good description, and that a wind of velocity  $\sim 6 \times 10^7 \text{ cm s}^{-1}$  is required to produce the observed filamentary structures. Furthermore, the kinematic zig-zag features only seem to form after about 30 Myrs, suggesting that the Perseus filaments are approximately this old.

In each case, the total mass removed from the cold cloud was of the order of  $10^9 M_\odot$ . However, the majority of this material is not in the filament, but is in the more amorphous and disrupted region behind the cloud. The material around the cloud is likely to have a low ionisation and is therefore not likely to be optically emitting.

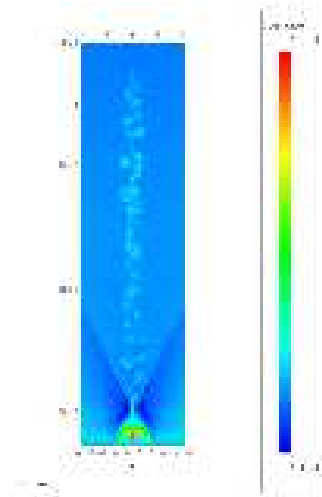


**Figure 14.** The density structure at 24 Myrs, for  $\eta = 10^3$  and wind velocity  $= 1.32 \times 10^8 \text{ cm s}^{-1}$ . The length scale indicates the distance from the cluster centre in kpc. The density scale shows the density in code units ( $\rho'$ ).

## 6 MOMENTUM TRANSFER FROM THE ICM

The kinematics of the filaments indicate that momentum transfer between the cool and hot phases of the ICM occurs. If there is a large enough quantity of cool gas, this could have important consequences for the flow of the hot phase. Momentum  $P$  is transferred from the hot ICM phase to a cloud at a rate

$$\dot{P}_{\text{clump}} = KA\rho_w(v_w - \dot{x})^2, \quad (26)$$

If the radius of the cloud is  $\sim 30 \text{ pc}$ , and  $(v_w - \dot{x}) \sim 10^{7-8} \text{ cm s}^{-1}$  then  $\dot{P}_{\text{clump}} \sim 10^{29-30} \text{ erg cm}^{-1}$ .

A rough estimate for the rate at which momentum is transferred from the external medium to the cloud's tail is

$$\dot{P}_{\text{tail}} = m_{\text{tail}}\ddot{x}_{\text{tail}}, \quad (27)$$

where  $m_{\text{tail}} = A\rho_{\text{tail}}l_{\text{tail}}$ ,  $\rho_{\text{tail}}$  is the density in the tail,  $\ddot{x}_{\text{tail}}$  is the typical acceleration in the tail, and  $l_{\text{tail}} = l_t$  is the length of the tail. Constant cross-sectional area, density, and acceleration along the tail are assumed. The acceleration can be approximated by  $\ddot{x}_{\text{tail}} = (\dot{x} - u)^2/2l_{\text{tail}}$  where  $\dot{x}$  is the

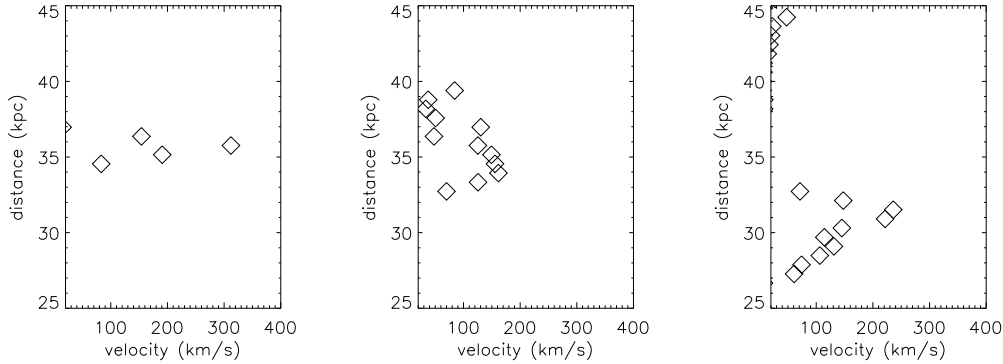


**Figure 16.** Velocity profile for case  $\eta = 10^4$  and wind velocity  $= 4.32 \times 10^8 \text{ cm s}^{-1}$ . Panels show data at 16, 23 and 38 Myrs. The length scale indicates the distance from the cluster centre. We have cut off the central  $20 \text{ km s}^{-1}$  to exclude points where there is no tail.

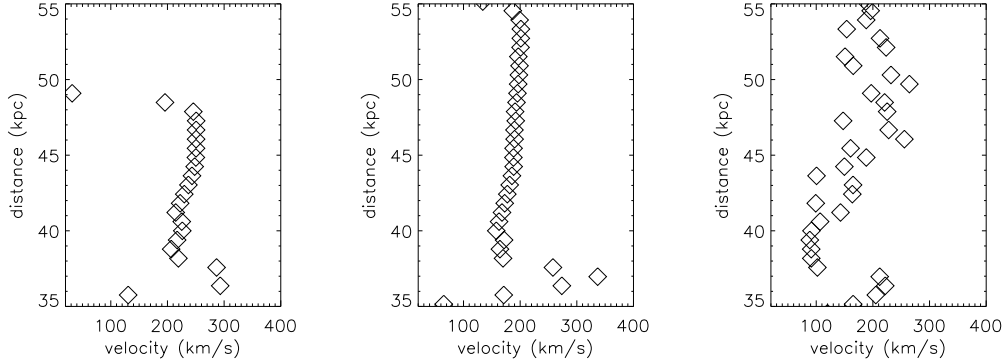


**Figure 17.** Velocity profile for case  $\eta = 10^3$  and wind velocity  $= 1.76 \times 10^8 \text{ cm s}^{-1}$ . Panels show data at 8, 12 and 20 Myrs. The length scale indicates the distance from the cluster centre. We have cut off the central  $20 \text{ km s}^{-1}$  to exclude points where there is no tail.

velocity of the clump, and  $u$  is the maximum velocity of the tail material. If the number density in the tail is about  $10 \text{ cm}^{-3}$ , the tail radius is about  $50 \text{ pc}$ , and the magnitude of  $|u - \dot{x}|$  is  $\sim 10^2 \text{ km s}^{-1}$ , then

$$\dot{P}_{\text{tail}} \sim 10^{32} \left( \frac{n}{10 \text{ cm}^{-3}} \right) \left( \frac{R}{50 \text{ pc}} \right)^2 \left( \frac{\dot{x} - u}{100 \text{ km s}^{-1}} \right)^2 \text{ erg cm}^{-1} \quad (28)$$

The corresponding rate at which systemic kinetic energy is transferred to the tail is  $\dot{E}_{\text{tail}} \sim \dot{P}_{\text{tail}} |u - \dot{x}|$ ,

$$\dot{E}_{\text{tail}} \sim 10^{39} \left( \frac{n}{10 \text{ cm}^{-3}} \right) \left( \frac{R}{50 \text{ pc}} \right)^2 \left( \frac{\dot{x} - u}{100 \text{ km s}^{-1}} \right)^3 \text{ erg s}^{-1} \quad (29)$$

If the energy dissipated as thermal energy were comparable to this and all of that thermal energy were radiated in the observed optical lines, about 100 tails would account for the observed optical luminosity of the NGC 1275 filaments.

The estimate above suggests that the tails are extremely massive  $\sim 10^8 M_{\odot}$ , though the mass of ionised material must be much lower (e.g. Hatch et al. 2007). This suggests that the filaments may consist of molecular material surrounded by a skin of ionised material.

We can compare the momentum transfer between the phases of the ICM, with that developed by an AGN jet, which may in turn drive a wind from the central galaxy. A jet injecting material at  $1 M_{\odot} \text{ yr}^{-1}$  with a velocity of 0.1

times the speed of light over a lifetime of 10 Myrs, has  $\dot{P} \sim 10^{50} \text{ g cm s}^{-1}$ . This can be compared to the total momentum transferred along the length of a filament by the wind  $\sim \dot{x} A l_{\text{tail}} \rho_{\text{tail}} \sim 10^{48} \text{ g cm s}^{-1}$ . This suggests that the momentum transfer to many tails could be important for dissipating the energy injected by an AGN in the ICM. In particular, since much of the cold material is located near the centre of the cluster, if this dissipation mechanism is significant, then it will increase the AGN heating efficiency in the central regions of the cluster. Without this obstructing cold material, more of the injected energy would be deposited at larger radii, thus failing to heat the central regions where energy is most needed.

To summarise this point it is worth reiterating that tails only seem to form if there is a significant outflowing wind - they are formed by the ambient wind dragging and accelerating material, transferring energy and momentum to the cold material. As a result they are probably a sign of activity in the central galaxy. This mechanism can provide a way of coupling the wind to the cold material. Given that the cold clouds are likely to proliferate near the cluster this means that the energy will be dissipated more centrally than in the absence of the cold material. As such, the cold material increases the effective opacity of the ICM to the outflowing wind.

To estimate this effect, let us assume that energy is

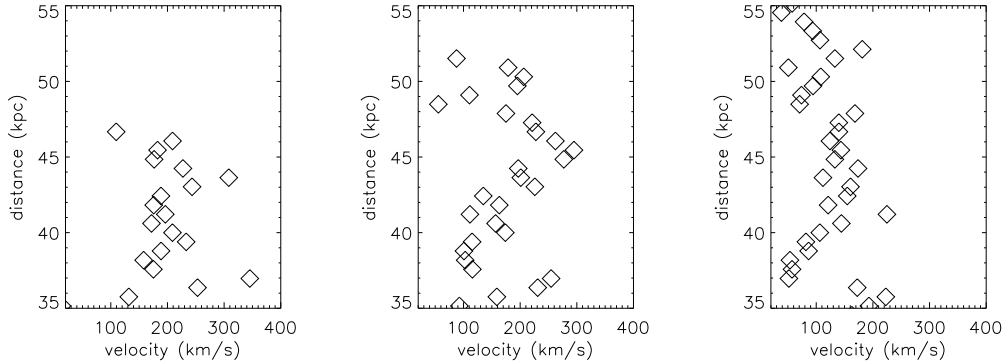


**Figure 18.** Velocity profile for case  $\eta = 10^3$  and wind velocity  $= 1.32 \times 10^8 \text{ cm s}^{-1}$ . Panels show data at  $0.9, 1.4$  and  $2.4 \times 10^7$  yrs. The length scale indicates the distance from the cluster centre. We have cut off the central  $20 \text{ km s}^{-1}$  to exclude points where there is no tail.

injected at a rate  $\dot{E}_{\text{in}}$ , the energy dissipation rate per tail is  $\dot{E}_{\text{tail}}$ , and there are  $N$  tails. The change in power of the wind, over a region in which there are  $N$  clouds, will be  $\Delta \dot{E} = \dot{E}_{\text{in}} - N \dot{E}_{\text{tail}}$ . Taking the derivative with respect to radius, and assuming that  $\dot{E}_{\text{tail}}$  is a constant we find,

$$\frac{d\dot{E}}{dr} = -\frac{dN}{dr} \dot{E}_{\text{tail}}, \quad (30)$$

where  $dN/dr$  is obtained from the spatial distribution of the clouds,

$$\frac{dN}{dr} = 4\pi r^2 n(r) \quad (31)$$

and  $n(r)$  is the concentration of clouds per unit volume. If we assume that the clouds are distributed similarly to the hot gas, in a  $\beta$ -profile, then

$$n(r) = \frac{n_0}{(1 + (r/r_0)^2)^\beta}, \quad (32)$$

where  $n_0$  is the central density and  $r_0$  is a scale length. Choosing  $\beta = 1$  means that equation (30) can be integrated analytically to give,

$$\dot{E}(r) = \dot{E}_{\text{in}} - N_0 \dot{E}_{\text{tail}} \left[ \frac{r}{r_0} - \arctan\left(\frac{r}{r_0}\right) \right], \quad (33)$$

where  $N_0 = 4\pi n_0 r_0^3$ . Therefore, the injected energy would be dissipated over a typical length-scale

$$r_{\text{diss}} \sim \frac{r_0 \dot{E}_{\text{in}}}{N_0 \dot{E}_{\text{tail}}}. \quad (34)$$

Given that  $r_0$  is probably a constant of the system, and  $\dot{E}_{\text{tail}}$  is also probably fairly constant, the important parameters are  $\dot{E}_{\text{in}}$  and  $N_0$ . For a moderate AGN outburst,  $\dot{E}_{\text{in}} \sim 10^{43} \text{ erg s}^{-1}$ , with  $\dot{E}_{\text{tail}} \sim 10^{40} \text{ erg s}^{-1}$  and  $N_0 \sim 1000$  (corresponding to a total cold mass of  $10^{11} M_\odot$ ), the dissipation length is of the same order as the scale-height of the cloud distribution. (This may be comparable to the scale-height of the ICM, but that is not clear. It is also possible that the clouds are more centrally concentrated than the hot ICM, but again, this is speculation.) For more powerful outbursts, a significant quantity of energy may be trapped, but the majority will still escape outside  $r_0$ .

It is worth noting that if there has been significant recent cooling (i.e. a deficit of heating) we may expect  $N_0$  to be larger, for a given system. For a given energy injection

rate, the energy will necessarily be dissipated closer to the centre than in an otherwise identical system where  $N_0$  is lower. As a result, the presence of cold gas may provide an additional feedback process that helps to trap energy in the central regions. This effect will be greater if there has been a recent deficit of heating, with the trapping effect being reduced in the absence of cold material.

This short derivation is, of course, a drastic simplification of real life. For example, in reality, the power dissipated in a tail is a reflection of the power of the incident wind, which will undoubtedly be a function of radius. However, it highlights the possibility that the production of filaments may be able to trap a fraction the energy injected by a central AGN.

## 7 GENERAL EXPECTATIONS FOR OPTICAL EMISSION-LINE FILAMENTS IN GALAXY CLUSTERS

The current study is centred on the Perseus cluster and concerns the interaction of material injected from one cloud into a hot flow unaffected by other clouds. A global consideration of the effects of a distribution of clouds on the hot flow out to  $\sim 10$  kpc would be required to investigate the problem more completely, and we plan to investigate such problems. However, a full answer would require the development of a detailed theory for the spatial and mass distributions of the clouds; given the state of the theory of our own interstellar medium this task would be very difficult.

The nature and number of filaments will depend on: a) the spatial, mass and velocity distributions of cold clouds at the onset of AGN activity; b) the rate at which the AGN deposits mechanical and thermal energy into its outflow and the asymmetry of these AGN outflows; c) the pressure, velocity, and density distributions of the hot intracluster gas at the onset of AGN activity; d) the gravitational potential of the galaxy. Below we consider, in sequence, how each of these could affect the filamentary structure.

a) If all other factors were the same, the total number of filaments and their combined optical luminosity would be roughly proportional to the number of clouds that could survive interactions with an outflow long enough for filaments to evolve. If the distribution of cloud masses were

identical in all clusters, the systems with the most cold gas would exhibit the most luminous optical emission from filaments. This is consistent with the findings of Edge (2001). The clouds which survive for longest are likely to be the most massive.

b) The number of massive clouds will depend on AGN activity. If the clouds are formed in a steady fountain flow, the rate at which material turns into clouds would be proportional to the outflow rate of hot material as measured near its the source. Roughly speaking, this mass outflow rate may be proportional to the mechanical luminosity of the AGN wind. In addition, the destruction rate of the clouds may also be proportional to the outflow rate. For example, a higher outflow rate could lead to a more rapid destruction rate of the clouds. Thus, it is possible that the number of clouds producing filaments would be fairly insensitive to the AGN mechanical luminosity. However, it would be cavalier to assume the locations at which clouds form, and the initial formation of the clouds, to be independent of the outflow rate.

c) The properties of the ICM could affect the initial mass function of the clouds. If significant, thermal conduction might establish the minimum lengthscale on which thermal instability grows. In hotter clusters, the minimum cloud mass would be higher, leading to a greater fraction of the clouds being formed with high masses. This would tend to increase the number of long filaments.

High ICM densities will lead to more rapid cooling and possibly a higher formation rate of clouds, and hence more filaments. However, given that AGN feedback is likely to be important, high cooling rates may cause strong AGN activity and thus reduce the cloud formation rate. The exact balance between heating and cooling seems to vary from cluster to cluster.

Clouds in the ICM may be so plentiful in the centre of a cluster that a bubble blown by the AGN becomes trapped near the cluster centre, preventing the formation of long filament. So, high ICM density need not necessarily result in the production of many filamentary tails.

d) The gravity of the central galaxy may play a role in limiting the size of the bubble mentioned in c). For example, the greater buoyancy may cause a bubble to detach sooner. Strong gravity may prevent an extended fountain or region of outflows. Even if it does not, it may limit the lifetimes of clouds as it would cause them to fall more rapidly.

In summary, the question about scaling concerns very complex issues. A very long concentrated program would be required to address them properly, and it is unclear how reliable the results of such a program would be.

## 8 SUMMARY

This work is intended mainly as a preliminary study into the processes that shape filamentary structures in the ICM, and not an exhaustive study. It is likely that there are many other processes such as magnetic fields, thermal conduction and viscosity that all play a role in the dynamics that produce the filamentary kinematics and morphology. However, we have concentrated on the basic hydrodynamic system and have found several interesting mechanisms that may go some way to explaining the properties of the observed filaments.

The first ensemble of simulations show that the long, relatively straight filaments at the centre of the Perseus cluster may be formed by the interaction of a wind with clumps of cold material. Flows of low Mach number winds generate structure in the filaments which may be comparable with observations. These results also suggest that the amplitude of the velocity fluctuations along the length of the filament grow with increasing density contrast between the cold material and the ambient wind. The morphology of the observed filaments suggests that the density contrast is large ( $\sim 10^4$ ). Interestingly, the fluctuations evolve with time providing a possible diagnostic tool for estimating the ages of filaments from observations. In this set of simulations, the best comparison with observations suggests filament ages of  $\sim 40$  Myrs in the Perseus cluster.

In a more realistic environment with spatially varying gravity, based on the Perseus cluster, filaments only form if the wind velocity is sufficiently large. If there is no significant wind, then the optical emission may be more amorphous, or more likely, filamentary on much shorter length scales. The morphology and kinematics suggests that a density contrast of  $\eta \sim 10^3$  may be more compatible with the observations, while the best agreement in the kinematic data occurs for  $\eta \sim 10^4$ . As a compromise it is possible that the real conditions lay somewhere between these two extremes. Alternatively, other physical processes could be important. It should also be noted that these were 2-d simulations, and a full 3-d study would really be required to find the model conditions that best match reality. Regardless of this, the results do point to a relatively narrow range of parameters providing possible information about the state of the ICM, and the age of the filaments. These results suggest that the cold material is of the order of  $10^4$  times denser than the ambient ICM, there is an outflowing wind of velocity of  $\sim 10^3$  km s $^{-1}$ , and that the filaments are approximately a few 10's of Myrs old.

The masses, and densities, of the filaments created by these simulations seem to be low compared with values presented in the previous section. The simulations produce filaments of  $10^6 - 10^7 M_\odot$ , while the crude estimates above suggested that  $10^8 M_\odot$  filaments might be more likely. It should be noted though, that the quantity of cold gas, in the simulated tail, is more than capable of producing the observed optical luminosity. The simulations also show a lot of cold, dense gas in the vicinity of the cloud itself.

We also highlight the possibility that momentum transfer between the ICM and cold clouds could be a dynamically important process in galaxy clusters. This process could effectively couple the energy and momentum of an outflowing wind to the cold material, thereby dissipating some of the energy injected by a central AGN. The presence of cold gas may therefore provide an additional feedback mechanism that traps energy in the central regions of clusters where it is most needed.

## 9 ACKNOWLEDGEMENTS

We acknowledge Professor John E. Dyson and Dr Nina Hatch for many useful discussions and the anonymous referee for helpful comments.

## REFERENCES

- Braine J., Wyrowski F., Radford S. J. E., Henkel C., Lesch H., 1995, *A&A*, 293, 315
- Burbidge E. M., Burbidge G. R., 1965, *ApJ*, 142, 1351
- Canto J., Raga A. C., 1991, *ApJ*, 372, 646
- Crawford C. S., Allen S. W., Ebeling H., Edge A. C., Fabian A. C., 1999, *MNRAS*, 306, 857
- Crawford C. S., Fabian A. C., 1992, *MNRAS*, 259, 265
- Donahue M., Mack J., Voit G. M., Sparks W., Elston R., Maloney P. R., 2000, *ApJ*, 545, 670
- Donahue M., Voit G. M., 1991, *ApJ*, 381, 361
- Dyson J. E., Pittard J. M., Meaburn J., Falle S. A. E. G., 2006, *A&A*, 457, 561
- Edge A. C., 2001, *MNRAS*, 328, 762
- Fabian A. C., Nulsen P. E. J., Canizares C. R., 1984, *Nat.*, 310, 733
- Fabian A. C., Sanders J. S., Crawford C. S., Conselice C. J., Gallagher J. S., Wyse R. F. G., 2003, *MNRAS*, 344, L48
- Falle S. A. E. G., 1994, *MNRAS*, 269, 607
- Falle S. A. E. G., Coker R. F., Pittard J. M., Dyson J. E., Hartquist T. W., 2002, *MNRAS*, 329, 670
- Forman W., Jones C., Churazov E., Markevitch M., Nulsen P., Vikhlinin A., Begelman M., Böhringer H., Eilek J., Heinz S., Kraft R., Owen F., Pahre M., 2007, *ApJ*, 665, 1057
- Hartquist T. W., Dyson J. E., 1988, *Ap. & Sp. Sci.*, 144, 615
- Hatch N. A., Crawford C. S., Fabian A. C., 2007, *MNRAS*, 380, 33
- Hatch N. A., Crawford C. S., Johnstone R. M., Fabian A. C., 2006, *MNRAS*, 367, 433
- Heckman T. M., Baum S. A., van Breugel W. J. M., McCarthy P., 1989, *ApJ*, 338, 48
- Johnstone R. M., Fabian A. C., 1988, *MNRAS*, 233, 581
- Murray S. D., Lin D. N. C., 2004, *ApJ*, 615, 586
- Nipoti C., Binney J., 2004, *MNRAS*, 349, 1509
- Pittard J. M., Dyson J. E., Falle S. A. E. G., Hartquist T. W., 2005, *MNRAS*, 361, 1077
- Pope E. C. D., Pavlovski G., Kaiser C. R., Fangohr H., 2006, *MNRAS*, 367, 1121
- Roediger E., Brüggem M., Rebusco P., Böhringer H., Churazov E., 2007, *MNRAS*, 375, 15
- Ruszkowski M., Enßlin T. A., Brüggem M., Heinz S., Pfrommer C., 2007, *MNRAS*, 378, 662
- Sanders J. S., Fabian A. C., 2007, *MNRAS*, 381, 1381
- Shapiro P. R., Field G. B., 1976, *ApJ*, 205, 762
- Vernaleo J. C., Reynolds C. S., 2006, *ApJ*, 645, 83